High Performance Cryogenic Radiators for James Webb Space Telescope

Randy A. Franck[1] and Anthony P. Gurule[2] and Pamela A. Brinckerhoff[3] and Thomas R. McCallan[4] and Michael Renbarger[5] and Andrew A. Brown[6]

Ball Aerospace Technology Corporation, Boulder, Colorado, 80301

The James Webb Space Telescope (JWST), scheduled to launch in 2018, relies almost exclusively on passive, cryogenic cooling for the telescope and instruments. The final stage of passive cooling is provided by 5 single stage cryogenic radiators. Three of these radiators have been manufactured by Ball Aerospace and represent the state of the art and provide unprecedented performance. The evolution of the requirements and design, and the resulting performance are discussed. The most mature performance data for Ball Infrared Black (BIRB™) coating is included, as well as specialized material property performance and structural properties.

Nomenclature

BATC = Ball Aerospace & Technologies Corp
BSF = Backplane Support Frame
CAD = Computer Aided Design
CNT = Carbon Nanotube Technology
CTE = Coefficient of Thermal Expansion
FIR = Fixed ISIM Radiators
GHe = Gaseous Helium
GSFC = NASA Goddard Space Flight Center
ISIM = Integrated Science Instrument Module
JSC = NASA Johnson Space Center
JWST = James Webb Space Telescope
K = *Kelvin*
L2 = JWST Orbit: Second Lagrangian Libration point
LN2 = Liquid Nitrogen
MIRI = Mid InfraRed Instrument
NASA = National Aeronautics and Space Administration
NIRCam = Near InfraRed Camera
NIRSpec FPA = Near InfraRed Spectrograph Focal Plane Array
NIRSpec OA = Near InfraRed Spectrograph Optial Assembly
NTE = Not To Exceed
NVR = Nonvolatile Residue

[1] Principle Engineer, Cryogenic and Thermal Engineering Department, 1600 Commerce St., Boulder, CO, 80301 MS RA6
[2] Department Head, Cryogenic and Thermal Engineering Department, 1600 Commerce St., Boulder, CO, 80301 MS CO7
[3] Engineer II, Cryogenic and Thermal Engineering Department, 1600 Commerce St., Boulder, CO, 80301 MS RA6
[4] Principle Engineer, Mechanical Engineering Department, 1600 Commerce St., Boulder, CO, 80301 MS RA6
[5] Staff Consultant, Materials and Process Engineering Department, 1600 Commerce St., Boulder, CO, 80301 MS RA6
[6] Principle Engineer, Mechanical Engineering Department, 1600 Commerce St., Boulder, CO, 80301 MS RA6

OCHC = Open Cell Honey Comb
OTE = Optical Telescope Element
OTIS = OTE and ISIM Assembly
PAC = Percent Area Coverage
QS = Quasi-Static Loads
TRL = Technology Readiness Level

I. Introduction

The James Webb Space Telescope (JWST) is a large space telescope that is to be launched later this decade. JWST is optimized to look at the universe in the infrared spectrum. In order to 'see' in the infrared wavelengths, the instruments suite and entire telescope have to reach deep cryogenic temperatures. Figure 1 shows the entire observatory. The major optical elements of the telescope and the sunshield are called out in the figure. Everything above the tennis-court-sized deployable sunshield is at cryogenic temperatures via a combination of 'open architecture' which exposes much of the system's surfaces (that are shielded from the sun) to a view of deep space, as well as direct cooling with cryogenic radiators. JWST will enable scientists to investigate the origins of the cosmos and life in the universe.

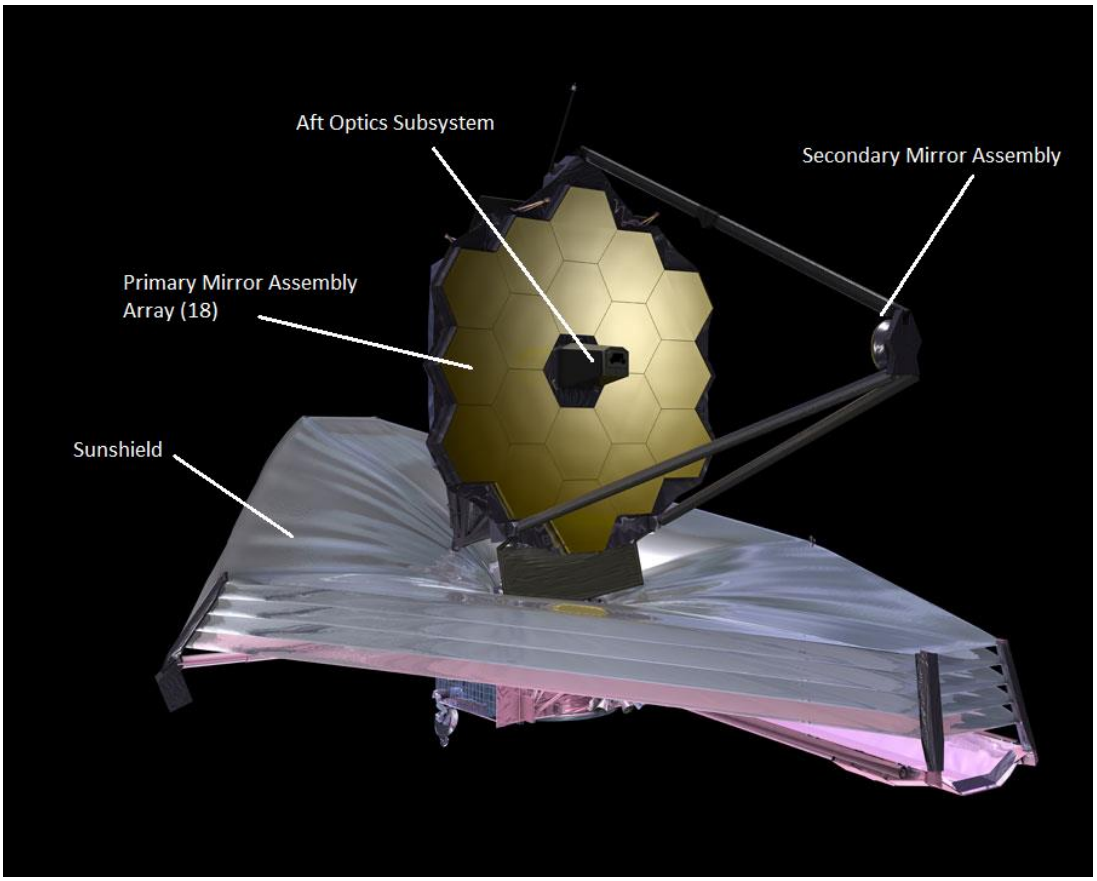

Figure 1. James Webb Space Telescope with Sunshield and Optical Elements Labeled.

The final stage of cooling for the science instruments, with the exception of the 6K MIRI detector, is provided by single stage radiators located 'behind' the primary mirror array and facing the anti-sun direction. This is the +V3 direction in the vehicle coordinate system. The combination of scale and passive cryogenic operational temperature is unique for cryogenic radiators, but most closely approached by the Spitzer Space Telescope, which used a cryostat for its primary detector cooling, and telescope housing coated with BIRB^{TM} that reached about 35K passively.

The JWST cryoradiators are thermally strapped to the instrument suite via 99.999% pure aluminum, mechanically compliant thermal straps. This minimizes the temperature rise from the cryoradiator to the instrument suite. Three of the radiators are 'fixed' and are the subject of this paper. The three Fixed ISIM Radiators (FIR) are

NIRSpec FPA, NIRSpec OA, and NIRCam. An additional two are Aft Deployable Infrared Radiators (ADIR), manufactured by Northrup Grumman Aerospace Systems. The suite of 5 cryogenic radiators are shown and labeled in Figure 2. This suite of passive radiators provides indefinite and reliable final stage cooling to the science instruments. This thermal design supports the mission life goal of greater than 10 years.

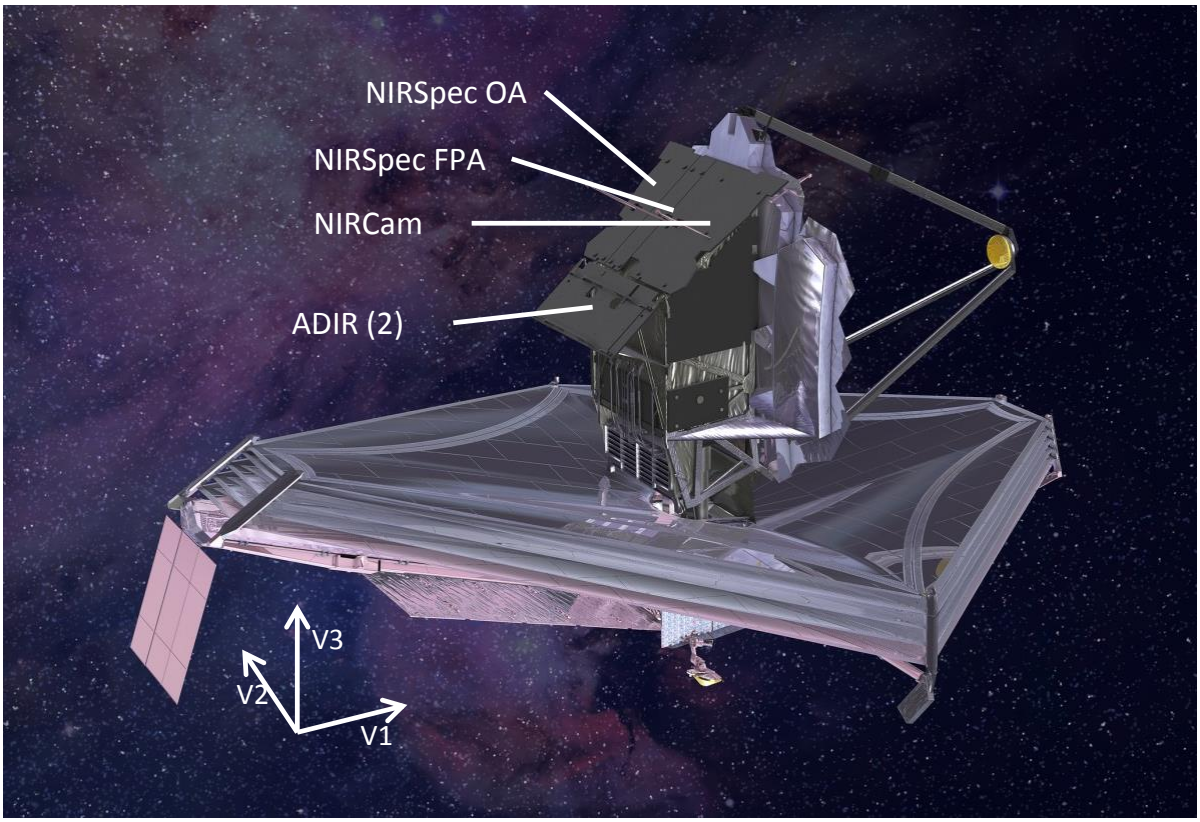

Figure 2. James Webb Telescope with the 5 Cryogenic Radiators, Labeled.

II. Evolution of Cryoradiator Requirements

The FIR occupy a finite area on the +V3 side of the observatory. Significant portions of the heat to be rejected by the radiators are system level 'parasitics'. Parasitics are not part of the instrument generated heat. These parasitics are accumulated from the surrounding hardware thermal environment at the instruments and along the thermal straps to the radiators. The complex system level thermal model predictions changed over time and there was some risk associated with locking down the area allocations to the 3 fixed radiators too early in the program. As a result, the allocation of this fixed area among the 3 radiators that occupy it changed over time. Some modular designs were considered for the radiators, so that they could be built and areas re-allocated later in the program. However, the inefficiencies and complexities of these designs soon became untenable. The radiators were then baselined back to more traditional designs, high purity aluminum facesheet honeycomb panels. The Integrated Science Instrument Module (ISIM) testing was originally baselined to include the radiators which would have driven the need date, but the ISIM tests were redesigned to simulate the radiators with q-meters, which gave both schedule relief to the final radiator requirements, as well as precise and heat based measurements to the ISIM at the radiator interfaces. Due to the deep cryogenic operational temperatures of the radiators, large areas are needed to dissipate relatively small amounts of heat. The ability of a 1m^2 perfectly black radiator staring at deep space to radiate heat is shown as a function of radiator operating temperature in Figure 3. The operational temperatures for the FIR range between 35K and 40K. Figure 4 shows the overall scale of the FIR in a dimensioned CAD image.

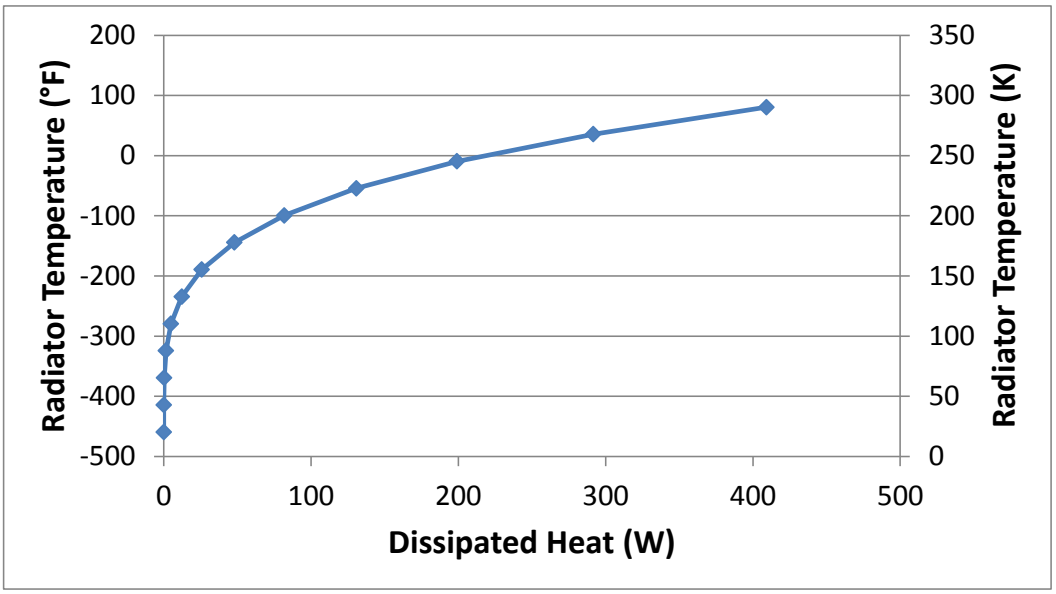

Figure 3. Dissipated Heat as a Function of Radiator Temperature for a 1m^2 Black Radiator.

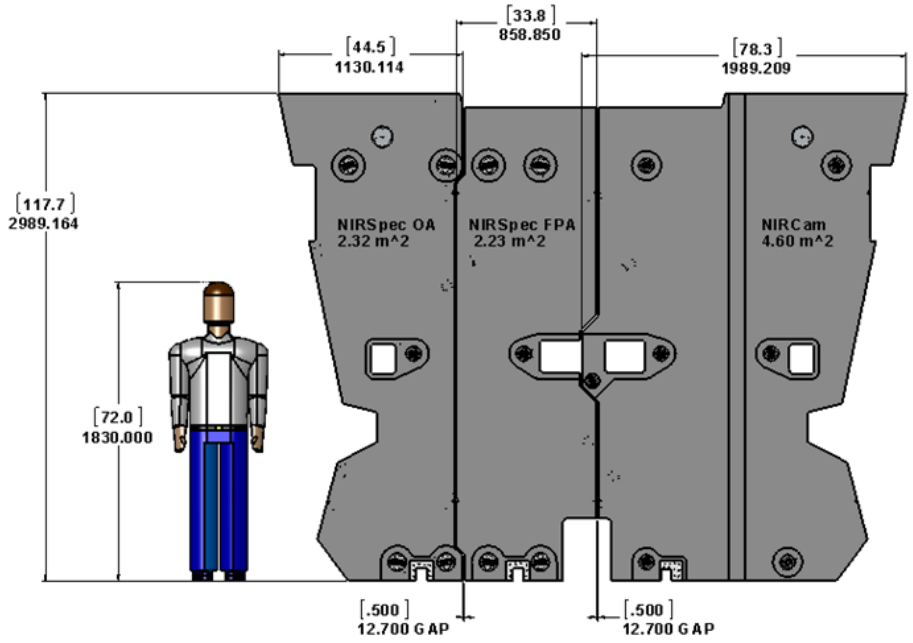

Figure 4. Dimensioned CAD Image of FIR. Dimensions in millimeters [inches].

At the beginning of the radiator program, the structural requirements included the basics: min frequency, QS design loads, acoustic environment, 25K survival, hot survival. Over time, the requirements evolved into a much more complex set which consisted of damping, mass, higher minimum frequencies, higher quasi-static design loads, acoustic, 25K survival for orbit and test, 410K hot survival for launch and ascent hot temperatures coupled with quasi-static loads, assembly loads consisting of local, global, and rotational misalignments during integration, BSF distortions during 25K cooldown on-orbit and in-test, and dissimilar material residual joint bolt loads.

The FIR were modified on a number of occasions to keep up with changing requirements including temperature, heatlift, launch and cryo structural loads and survival temperatures. As the thermal and structural requirements

settled, this period was also used to optimize the design and do risk reduction work on aspects of the design that were less mature or could be optimized.

The final set of requirements included the aforementioned structural requirements, area, heatlift vs. maximum temperature, venting, backside emissivity, min/max survival temperatures and temperature and conductance requirements at the mounting interfaces. Additionally, launch loads at the mounts and the heatstraps were specified individually along with the loads imparted from the radiator mounts into the structure due to these loads, CTE loads and integration loads were constrained to the capabilities of the flight Backplane Support Frame (BSF) which was already under construction.

III. Evolution of Cryoradiator Design

The design baselined high purity aluminum 1100 facesheet honeycomb core composite panels. Numerous trades were performed with various facesheet materials in order to see if mass reductions and a better CTE match to the low CTE BSF could be realized. In the end, aluminum still outperformed the alternative materials when considering the entire risk profile. However, the final choice of facesheet material was changed from Al1100 to Al1350. Al1350 is nominally only 0.5% more pure (99.7% pure actual) than Al1100, but that small increase in purity produces a 2X increase in conductivity at the operating temperature range of the radiators, Figure 5. This material conductivity performance allowed for lighter facesheets as well the locations of the heat strap interfaces to the edges of the radiators with minimal loss in radiator fin efficiency.

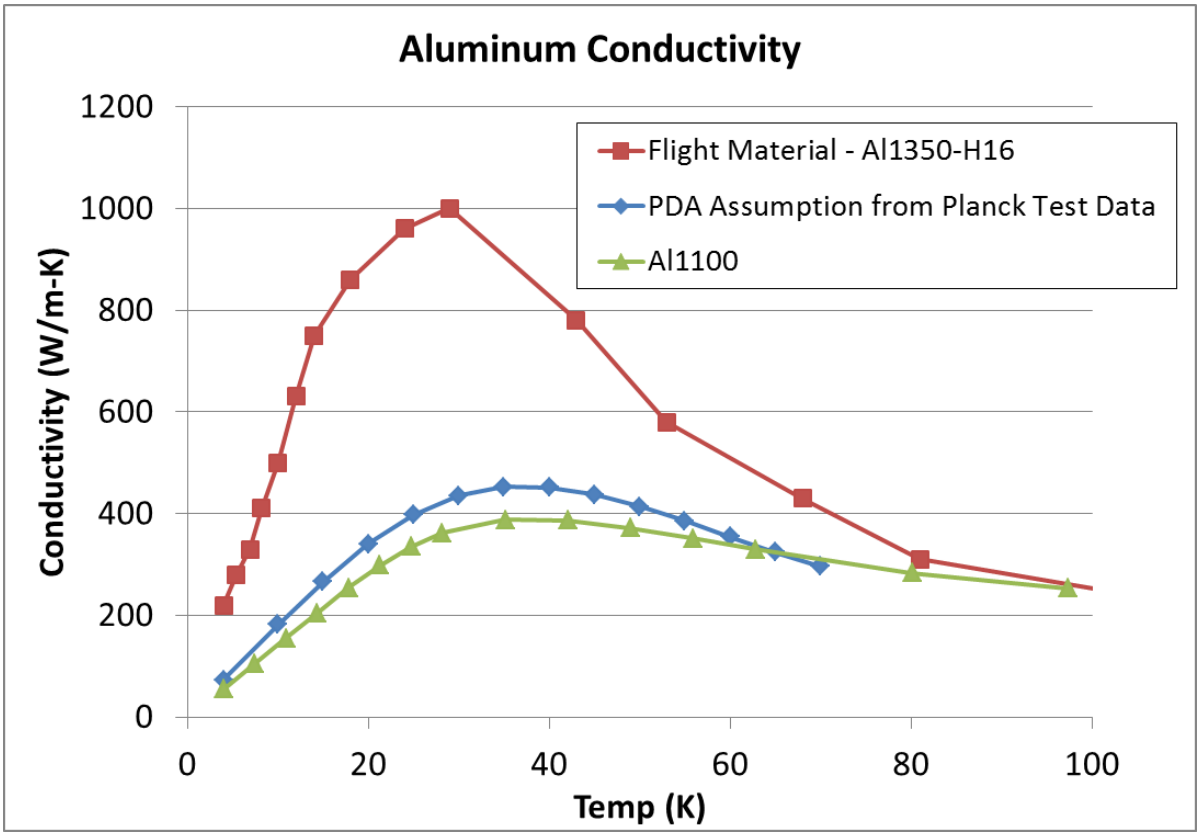

Figure 5 Comparison of the Flight Aluminum (1350) Conductivity to Traditional Al1100.

Challenges with producing and procuring the Al1350 sheet stock were overcome. A facesheet joint design for the larger radiator which exceeded the maximum available sheet width was designed. The facesheets were chem-milled in order to provide the maximum thermal performance with the minimum mass. Local areas around the mounting locations were thicker to provide additional strength for various structural loads. Figure 5 shows two of the facesheets after etching operations.

Because the Aluminum panel was the final design choice, emphasis was put on the design of the radiator composite flexure mounts including their locations relative to each panel's center mount and their cross sectional geometry mainly driven by the 25K cooldown loads relative to the low CTE BSF structure the FIR mount to. Due to the large span of the radiators and underlying BSF beam locations, a limited range of possibilities existed to locate the mounts. At a specific point in the design evolution, it was required to freeze the locations of the mounts due to the BSF build, even while anticipated area re-allocations between the 3 radiators were pending. At the time, the mount locations and geometry were optimized to balance both flexibility (for cooldown) and stiffness (for launch) for the given radiator design areas. 25K loading drove the composite flexure blade free height and bonded overlaps, while QS design loads drove the flexure blade thickness for buckling and width for bond and blade stresses. 3 unique flexure cross sections were utilized for the radiators. The locations of the mounts were important for both 25K loads and QS launch loads. Additional considerations which affected blade thicknesses included utilizing a heritage ply set for the balanced/symmetric composite in order to accurately predict thermal and mechanical properties early in the design. Of course, the need for composite flexures was driven by the thermal performance requirement of the radiators. Fortunately, the composite system chosen was well understood and still allowed the team to meet the stringent and evolving structural requirements.

Prior to the radiator's final PDA, mass became an important design driver at the system level. The team was tasked to optimize the design and remove as much mass as possible while maximizing thermal performance. Removing mass while maintaining areas required increases to the QS design accelerations to cover higher expected acoustic loads. Also, a sinusoidal launch event drove the minimum frequency requirement higher. Due to these changes, each radiator's center post design was revisited. The center post went from a monoball strut end design to a fixed composite tube. The fixed tube drove the lateral panel frequency above the minimum requirement and assisted in carrying launch loads. Drawbacks to implementing the post design change included increasing the hot and cold thermal loads into the BSF as well as the global integration loads on the flexures.

Risk reduction testing played a very important role in the success of the radiators. Test types could be broken down into the following categories: material characterization, subcomponent, engineering development units, and flight.

Measured curves from room temperature to below 20K were developed for the key flight thermal materials; the facesheet conductivity, and the BIRB^{TM} cryogenic emissivity. Many other aspects of BIRB^{TM} were also measured early in the program[1], and BIRB^{TM} cryogenic emissivity is discussed below and in several more recent publications[2,3,4]. The thermal conductivity performance of Al1350 is discussed above.

Test derived mechanical and thermal properties at room temperature, 25K, and 410K were used to tune structural FEM properties to allow for accurate predictions and write margins of safety. Final structural models were correlated and verified through comparison to modal survey tests of individual panels. Material characterization included composite laminate tension, compression, shear, bearing and CTE. Subcomponent tests were comprised of composite/Ti lap shears, Al/Al lap shears, and Al facesheet/core 4 point bend beams and normal direction samples. Engineering development units of the composite/Ti flexures and center post mount designs were built to test static strength capacity; flight-like honeycomb panels and particle dampers were also assembled to measure damping performance. Flight tests included NDE of flight panels, separate static proof tests on all composite/Ti flexures and center post mounts as well as on the flight panels, assembly level modal tests, and reverberant chamber acoustic tests.

Figure 6 FIR Facesheets After Milling Operations.

As mentioned above, the design incorporates a coating developed at Ball Aerospace for and first flown on the Spitzer space telescope. Radiator coating trades were performed over the course of the program, including investigations into Carbon Nanotube Technology (CNT) and painted Open Cell Honeycomb (OCHC) which both fell short of BIRB^{TM} when looking at combined weighted mass, cleanliness, emissivity, and TRL performance. BIRB^{TM} produces exceptional cryogenic performance not only for emissivity, but for adhesion, CTE accommodation, cleanliness, electrostatic dissipation, and mass. Through the course of JWST, the coating was further qualified, including new application facilities, optimization for lightweighting, cleanliness, vibration and thermal performance. In parallel, new test methodologies for accurately measuring the cryogenic emissivities of coatings were developed and implemented. This enabled the program to confidently assess primary coating performance metric (cryogenic emissivity) vs. parameters such as coating areal density (kg/m^2). The cryogenic emissivity test methodologies have been described in Reference 3. The flight coupon measured emissivity, with uncertainty bars, of the BIRB^{TM} configuration is shown in Figure 7.

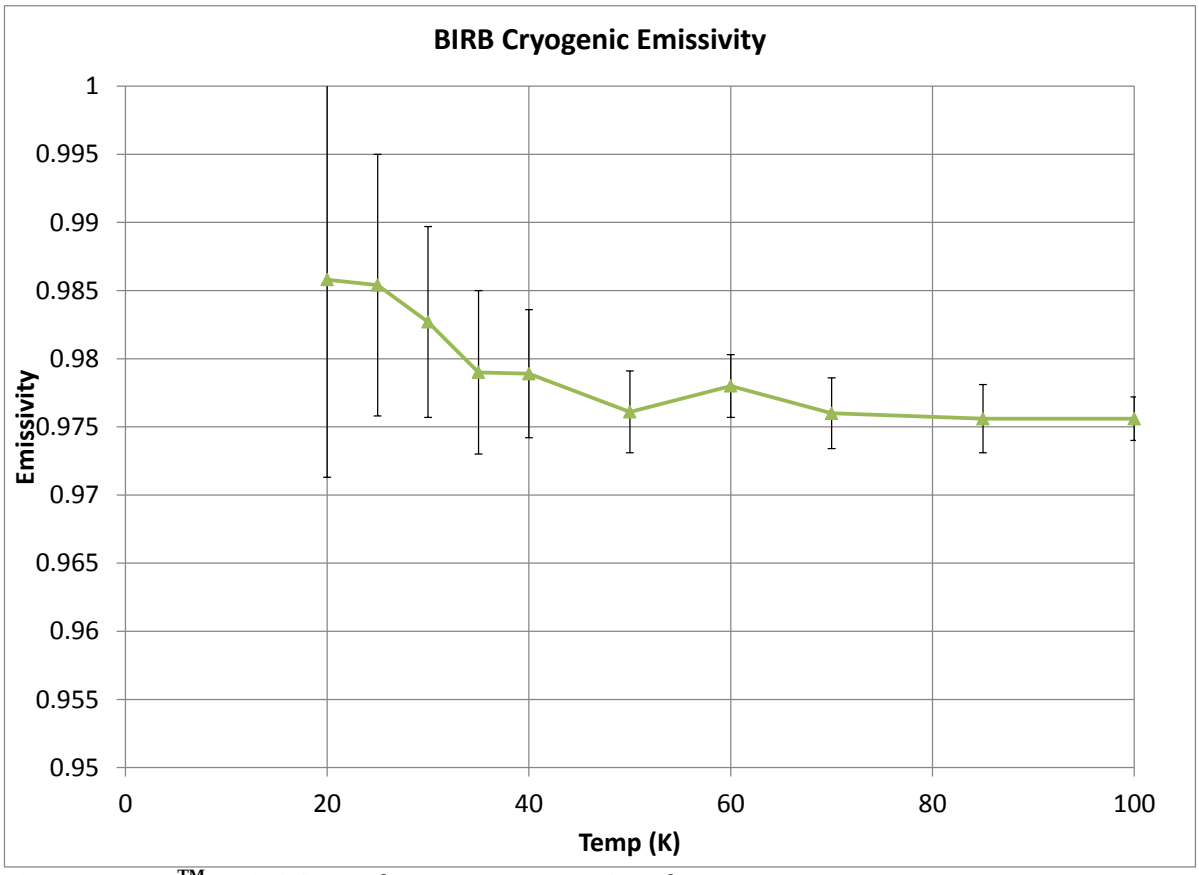

Figure 7 BIRB™ Emissivity Performance as a Function of Temperature.

The radiator final assemblies included flight temperature sensors, vent path accommodation, thermal strap interface pad, and particle dampers. The final design also maximized the coated surface area, and accommodated a difficult system integration strategy with the mounting features. Pictures in Figures 8 and 9 show two of the radiators during final assembly.

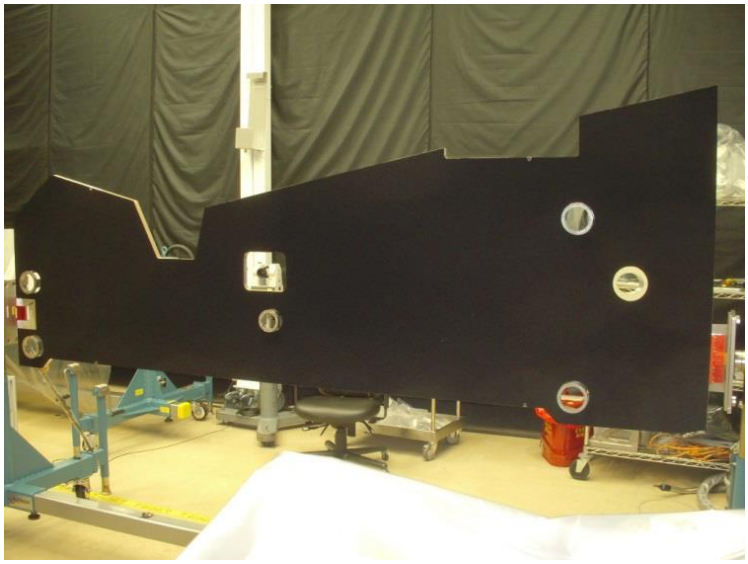

Figure 8 The NIRSpec OA Radiator During Build

Figure 9 The NIRSpec FPA Radiator During Build.

IV. FIR Performance

In order to verify the FIR thermal performance, the radiators were subjected to thermal balance testing. The thermal balance testing consisted of taking each radiator to its flight specification temperature environment in a space-like environment. To accomplish that, the radiators were placed in a thermal vacuum chamber at Ball Aerospace for this testing. The chamber had been fitted with a helium cooled shroud, which was able to attain 13K temperatures. It was important to have a cold source that could achieve such cold temperatures for the best representation of the space background, which reduces uncertainty in the test. To further simulate space, a sub-enclosure using BIRB^{TM} the create a near-black effect was placed around the radiator. The radiators were supported in the chamber by their flight flexures, which were controlled to their flight predicted temperatures via heaters. The test assembly with 2 of the FIR enclosed by the simulator is shown in Figure 10.

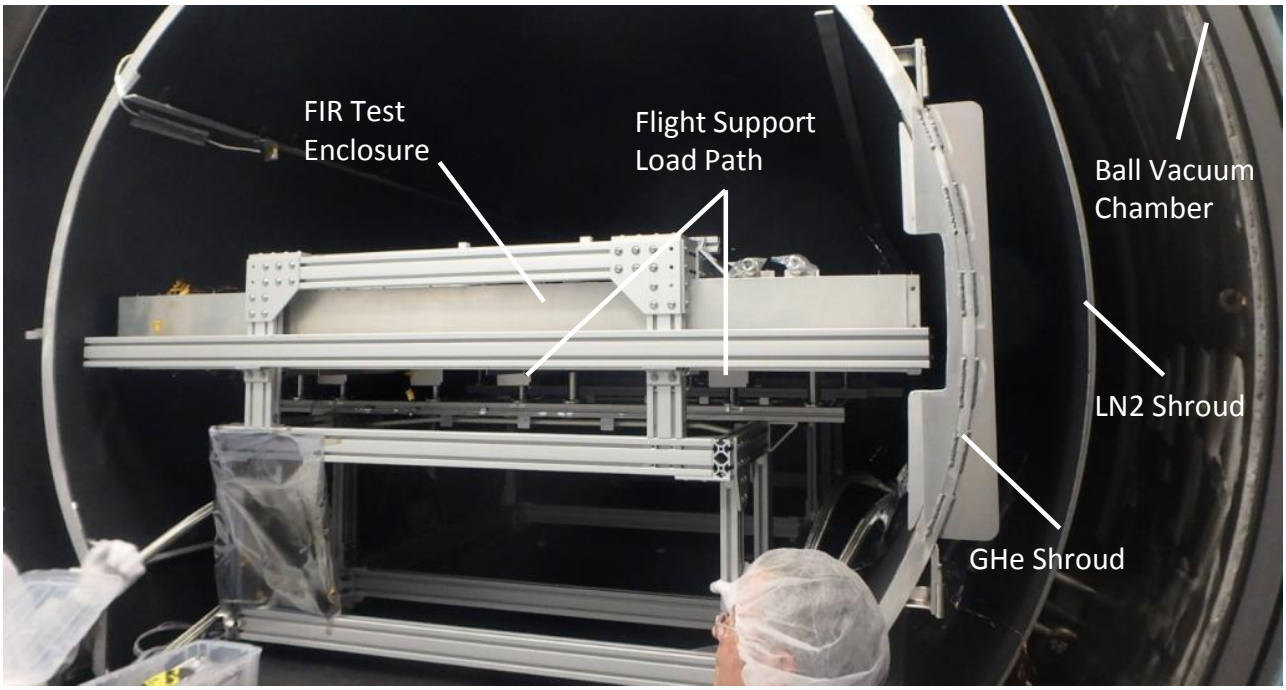

Figure 10 The FIR Thermal Test Environment.

With the space-side of the radiators facing the cold space-like environment, and the opposite side facing a black environment at the observatory sink temperature, a heat load or temperature was specified at the radiator's heat strap interface, and then the radiators were allowed to reach steady state conditions in that environment. Once the heat rejection from the radiator to the space environment had less than 1.5% of its radiating capability remaining, as determined by extrapolation of the current heat load rejection, then thermal balance was achieved. With the thermal balance data for each radiator, the thermal model was correlated to ensure the model accurately predicted the radiator's behavior in the testing environment. The correlated thermal model was then used to verify the flight performance requirements.

The performance of the FIR in many areas is beyond expectations and represents the state of the art for large single stage radiators operating at cryogenic temperatures. Below is a list of performance metrics and the achieved values for the FIR:

- Total Areal Density including mounting system (Kg/m^2)
  - NIRCam: 8.3, FPA: 10.6, OA: 11.3
- BIRB™ Areal Density
  - 0.65Kg/m^2
- Operational NTE Temperature at heatstrap I/F (K)
  - NIRCam: 39.58, FPA: 37.5, OA: 39.23
- Thermal margin against requirements after uncertainty (%)
  - NIRCam: 25.3, FPA: 19.9, OA: 27.3
- Radiator Fin Efficiency (%)
  - NIRCam: 94.9, FPA: 97.6, OA: 96.2
- Increase in damping averaged over the first 6 modes for each (demo) panel (% critical)
  - NIRCam: 2.54, FPA: 2.72, OA: 3.61
- CTE accommodation:
  - Up to 0.206 inches at heat strap and up to 0.245 inches at flexure mounts. NIRCam only, up to 0.336" at corner.
- Modal Characteristics
  - All radiators, first mode > 32Hz
- Induced forces at mounting locations:

- All below specified allowables as verified with acoustic testing

- Survival temperatures:
  - Minimum= 20Minimum= 25K, Maximum = 410K
- Contamination Control:
  - All three cryo radiators met their contamination control requirements of 0.04 PAC for particles and 1.0 mg/0.1m2 for NVR, equivalent to level 330A per IEST-STD-CC1246E. Table 1 presents the measured cleanliness levels at delivery:

FIR Panel Cleanliness at Delivery			Requirement
PAC	NIRCam	0.01413	0.04 as measured by fallout during acoustic test
	NIRSpec OA	0.00873	
	NiRSpec FPA	0.01029	
NVR (mg/0.1m^2)	NIRCam	0.0944 ± 0.0128	1
	NIRSpec OA	0.0940 + .0.0170	
	NiRSpec FPA	0.0998 + 0.01442	
	Flexures, Center Posts, and Bolts	<0.2	

Table 1. FIR PAC and NVR Performance.

One of the most compelling performance metrics to see how closely the FIR performance data land to the theoretical limit of thermal performance. The FIR are called out and shown in Figure 11. The survey of radiators are plotted as points, as a function of area divided by heat rejection capacity. These points are overlaid on a series of curves that shows how the fraction of parasitic heat affects the Area/Capacity metric. The FIR benefit from the L2 orbit as well as the cooled open architecture of JWST to keep the fraction of parasitics low. Note that the FIR, operating near 40K, approach the theoretical limit of radiator performance, even while achieving the lowest temperatures of the family of cryo-radiators plotted.

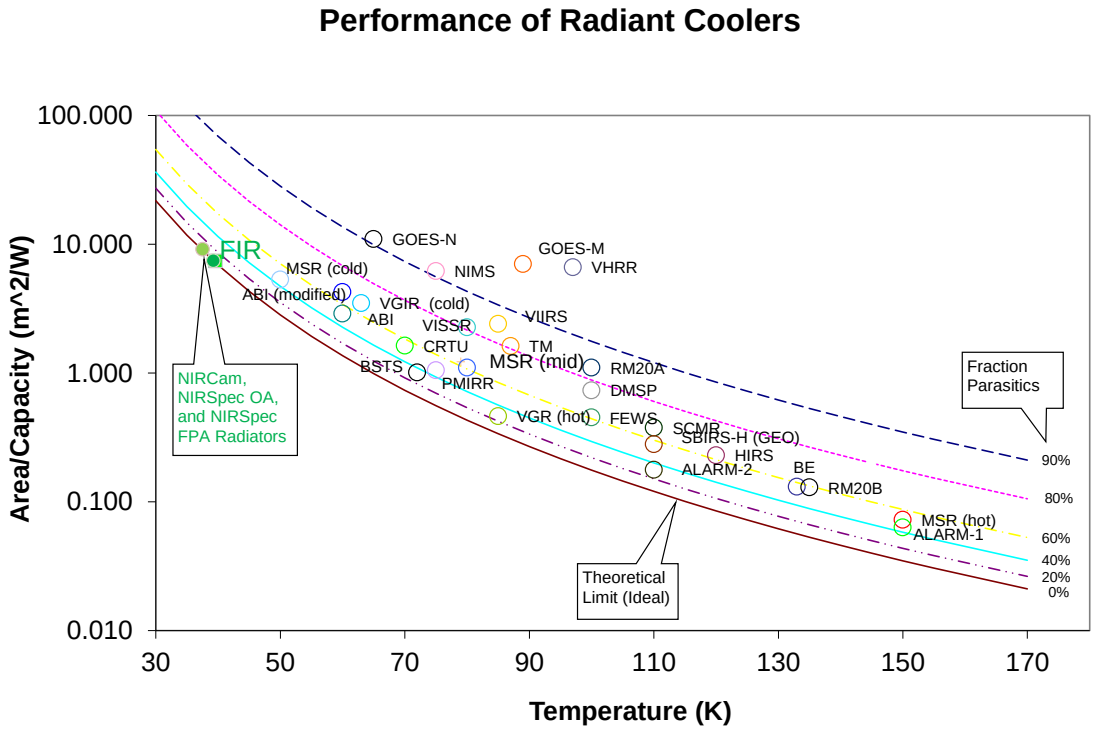

Figure 11 Performance of Radiant Coolers with FIR Included. Graph adapted from the Satellite Thermal Control Handbook, Vol II: Cryogenics, Figure 6.13[5].

V. Conclusion

The structural challenges of designing these large panels to accommodate a largely constrained and highly sensitive telescope structure cannot be overstated. However, the delay in the final radiator design, relative to observatory structure design and evolving thermal requirements, was critical in reducing the thermal performance risk of the key passive thermal features of the observatory and maximizing their performance.

The JWST FIR represents the state of the art in deep cryogenic radiator technology, approaching the theoretical limits of performance. The FIR enable JWST to fulfill the majority of its science objectives with reliable and long lasting passive cooling.

Acknowledgments

The authors would like to acknowledge the engineers, technicians and supportive management within Ball Aerospace, and across the program, past and present, who have contributed to this effort.

Figure 12 Ball FIR Team Members Posing in Front of the NIRCam FIR.

References

[1]Renbarger, M., "Properties of Ball InfraRed Black, a new cryogenic thermal control coating", *SPIE 7794, Optical System Contamination: Effects, Measurements, and Control* 77940F, San Diego, CA; doi:10.1117/12.858575; http://dx.doi.org/10.1117/12.858575.

[2]Franck, R.A., and Renbarger, M., "Cryogenic Emissivity Properties of Ball Infrared Black," *Advances in Cryogenic Engineering* 57B, Edited by J. G. Weisend et al., AIP, New York, 2012, pp 1497 - 1504.

[3]J. Tuttle, Edgar R. Canavan, Michael DiPirro, Xiaoyi Li, Randy Franck et al., "A High-Resolution Measurement of the Low-Temperature Emissivity of Ball Infrared Black," *Advances in Cryogenic Engineering* 57B, Edited by J. G. Weisend et al., AIP, New York, 2012, pp 1505 - 1512.

[4]Tuttle, Jim; Canavan, Ed; DiPirro, Mike; Li, Xiaoyi; Franck, Randy; Renbarger, Mike; Copp, Tracy; Hahn, Matt, "The area-density-dependence of Ball IR Black's low-temperature emissivity", 2014, *Cryogenics*, Volume 64, p. 240-243.

[5]Donebedian, M. (ed.), *Spacecraft Thermal Control Handbook, Volume II: Cryogenics*, The Aerospace Corporation, El Segundo, California, 2003, pp. 107-112.